ELSEVIER

Contents lists available at ScienceDirect

Journal of Power Sources

journal homepage: www.elsevier.com/locate/jpowsour



Short communication



Ni-rich $LiNi_{0.88}Mn_{0.06}Co_{0.06}O_2$ cathode interwoven by carbon fiber with improved rate capability and stability

Dong Ren¹, Yao Yang¹, Luxi Shen, Rui Zeng, Héctor D. Abruña ³

Department of Chemistry and Chemical Biology, Baker Laboratory, Cornell University, Ithaca, NY, 14853-1301, United States

HIGHLIGHTS

- LiNi_{0.88}Mn_{0.06}Co_{0.06}O₂/carbon fiber composite as the Ni-rich cathode material.
- Achieved a specific capacity of 212 and 137 mA h/g at 0.2 and 10 C, respectively.
- The superior performance of CF-NMC was ascribed to the faster ionic/electron diffusion.
- Structures were characterized by atomic-scale transmission electron microscopy.

ABSTRACT

Developing high-energy and high-power lithium-ion batteries represents the key challenge for electric vehicles. In this work, Ni-rich LiNi $_{0.88}$ Mn $_{0.06}$ Co $_{0.06}$ O₂ particles were synthesized by a facile co-precipitation method and interwoven by carbon fiber network (CF-NMC) as the cathode in lithium batteries. The CF-NMC material demonstrated superior electrochemical performance, relative to the pristine NMC, with an exceptional specific capacity of 210 mA h/g at 0.2 C and rate capability of 137 mA h/g and 95 mA h/g at 10 C and 20 C, respectively. These results not only provide further insights into the reaction mechanism but also illustrate a rational direction to synthesize practical Ni-rich cathode materials for Li-ion batteries and improve their high-power performance.

1. Introduction

A demand for high-energy and high-power lithium-ion batteries (LIBs) is increasing dramatically for large-scale applications including hybrid electric vehicles and fully electric vehicles [1,2]. However, their limited rate capability, moderate cycling life, and the high cost of electrode materials have precluded the development of LIBs for these applications. From a general point of view, high-energy and high-power LIBs can be achieved by using high-capacity and high-rate electrode materials, respectively. Lithium cobalt oxide (LCO), the most widely employed cathode material in consumer electronics with a relatively low practical capacity of \sim 150 mA h/g, is limited in use by the high cost of cobalt, safety issues and its high toxicity [3]. Among the commercially available candidate cathode materials for LIBs, Ni and Mn substituted compounds layered lithium nickel manganese cobalt oxides (NMC) have been widely explored since the introduction of Ohzuku's LiNi_{1/3}Mn_{1/3}. Co_{1/3}O₂ [4-6]. However, the instability of delithiated Li_xNiO₂ and LiMnO_2 has limited their use in electric vehicle and hybrid electric vehicle applications. The electronic conductivity and structural stability

of NMC compounds are also lower than those of LCO, thereby negatively affecting rate capability and cycling performance, respectively [7,8]. Different compounds with varying ratios of the three transition metals have been studied, but it has still not been possible to demonstrate stable high rates with conventional electrodes [9].

The discharge capacity of NMC materials is generally determined by the Ni content, as Ni is the major redox species (Ni^{2+}/Ni^{4+}) [10,11]. Thus higher Ni content (Ni>0.8) cathode active materials guarantee a high specific capacity [12–16]. As a result, a high energy density can be obtained. However, NMC cathode materials with higher Ni content (Ni>0.8) have shown poor rate capability, poor cycling life and poor thermal stability, due to structural instabilities [17]. Many efforts to enhance the conductivity of layered structures, that improves the rate performance, have been undertaken. Carbon coatings have been shown to be a successful pathway to ameliorate limited electronic conductivity [18–20]. Some nanoscale materials have also been used to improve rate performance by shortening lithium diffusion paths [21]. But, unanticipated side reactions, caused by the extra surface area from nanomaterials have impaired cycling life [22]. Surface coatings with stable

E-mail address: hda1@cornell.edu (H.D. Abruña).

^{*} Corresponding author.

¹ D. R. and Y. Y. contributed equally to this work.

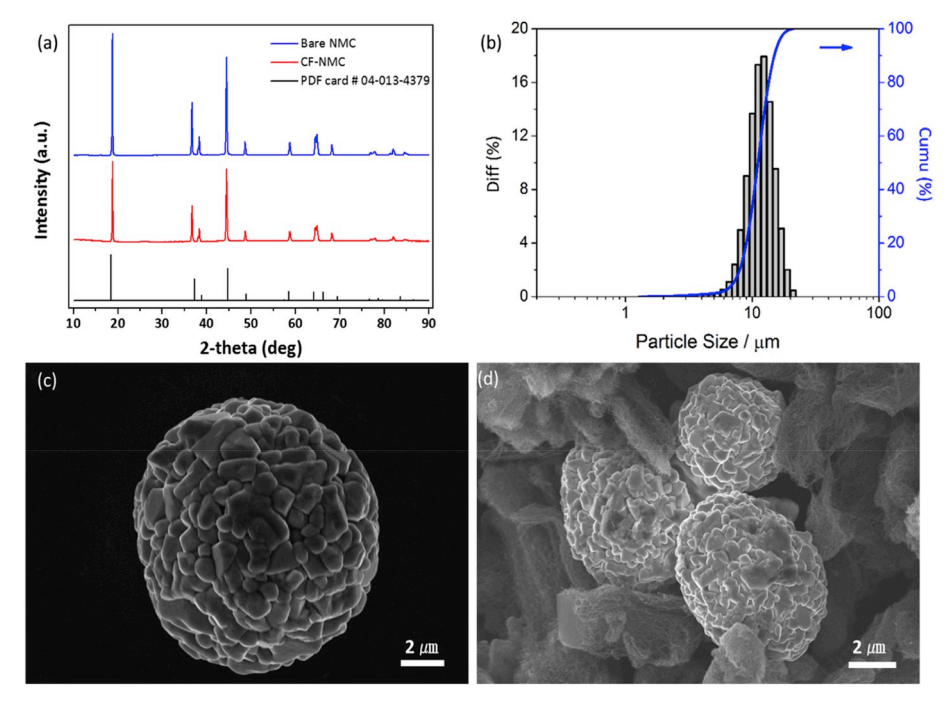


Fig. 1. (a) XRD patterns of pristine NMC and CF-NMC composite, compared with reference XRD of $LiNi_{1/3}Mn_{1/3}Co_{1/3}O_2$. (b) Particle size distribution of pristine NMC. (c) SEM image of pristine NMC. (d) SEM image of CF-NMC.

transition metal oxides have been employed to protect the surface, resulting in a longer cycling performance [23–25]. Nonetheless, the electronic conductivity will be reduced if the coating is an insulating material. To overcome the issues of high capacity Ni-rich cathodes while retaining excellent rate capability and long cycling life, rational design strategies are urgently needed. There is no prior literature of the simple application of bulk carbon fibers on greater Ni content NMC cathodes, and how the composite affects power and energy densities, and cycling performance.

2. Results and discussion

Fig. 1a presents the XRD patterns of our pristine Ni-rich NMC and the composite CF-NMC cathode materials. The sample yielded a well-defined and impurity-free single phase, and the reflections matched a hexagonal $\alpha\textsc{-NaFeO}_2$ type structure (space group R-3mH) [26]. The pristine NMC showed a XRD pattern and calculated lattice parameters nearly same as the CF-NMC, indicating the addition of carbon fiber did not alter the structure of NMC (Table S1). Additionally, the split between the (108)/(110) and (006)/(102) and peaks, respectively, indicated a good layering structure [27]. The lattice parameters of Ni-rich NMC were calculated based on the (003) and (104) peaks at 18.82° and

44.48°, respectively (a = b = 2.876 Å, c = 14.138 Å. cell volume, V = 101.24 Å). The peak intensity ratio of (003)/(104) can serve as a reliable indicator for the degree of cation mixing (Ni²⁺ occupancy on Li⁺ sites) in the layered oxide. Generally, when the intensity ratio of (003)/(104) is higher than 1.2, the degree of cation mixing is low, and the sample has a more well-defined layered structure [28]. Our Ni-rich NMC sample had a high value (1.23) of the (003)/(104) peak intensity ratio and, thus, a low value of cation mixing, which benefits the Li ion mobility upon charging and possibly contributes to a higher rate performance. As shown in Fig. 1b, the particle size distribution is defined as (D90-D10)/D50, in which D50 indicates a particle diameter that is larger than 50% of the total particle, while D90 and D10 represents the particle diameters that are larger than 90% and 10% of the total particles, respectively. The pristine NMC particle size (D50) was 11.69 µm with a narrow span of 0.62 μm, which could possibly contribute to a higher capacity at high C rates. SEM image in Figs. 1c and S1 showed that pristine NMC particles were composed of smaller primary particles. Benefitting from the well-controlled synthesis, the particles have a narrow size distribution with an average size of about 12 µm, which is consistent with the D50 value. Figs. 1d and S2 showed that the CF-NMC material was well embedded in the carbon fiber, which served as a highly efficient conductive network and facilitated

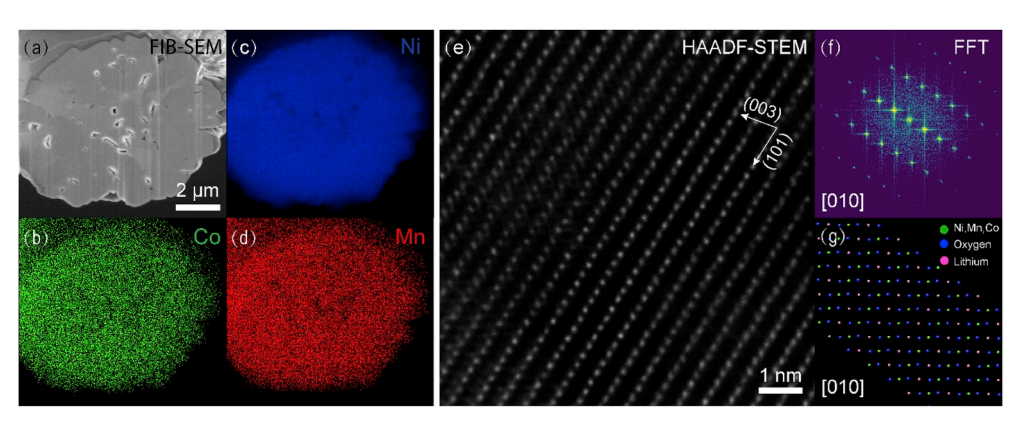


Fig. 2. (a) Cross-section SEM image of a Nirich NMC with a thickness of 1 μ m prepared by focused ion beam (FIB). (b–d): EDX elemental mapping of Co (b), Ni (c), Mn (d), respectively for the NMC lamella in (a). (e–f) HAADF-STEM image and the Fourier transform of an ultrathin NMC cross section showing atom columns with (003) and (101) d-spacings with an angle of 79.5° on the [010] zone axis. (g) The corresponding crystal model shows the projection of layered structure of transition metals in the [010] direction of the hexagonal crystal structure.

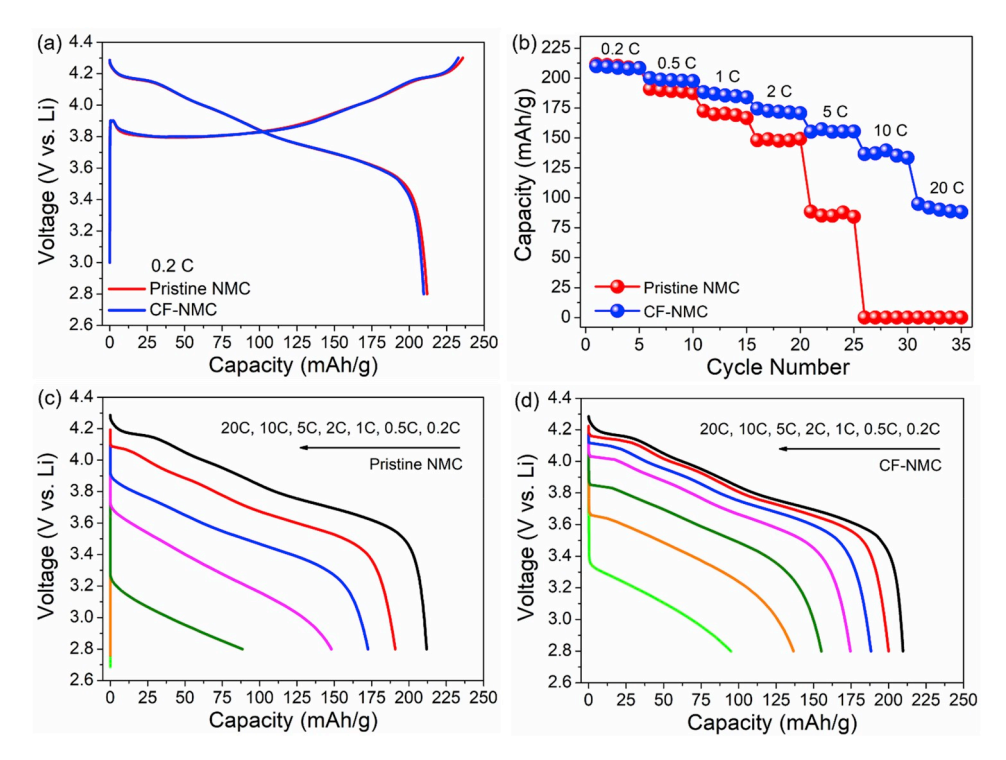


Fig. 3. (a) Initial charge—discharge profiles of CF-NMC and pristine NMC cells at 0.2 C between 2.8 and 4.3 V. (b) Rate performances of CF-NMC and pristine NMC cells from 0.2 C to 20 C. (c) Discharge profiles of a pristine NMC cell from 0.1 C to 20 C. (d) Discharge profiles of a CF-NMC cell from 0.1 C to 20 C.

lithiation/delithiation processes of NMC.

To better understand the microstructure of our NMC material, we employed focused ion beam (FIB) to mill a spherical NMC particle into a thin cross section (Fig. 2). Fig. 2a exhibited a NMC lamella, with a thickness of 1 µm. It has a dense internal microstructure with multiple crystal grains and several small pores. This structure could arise from the fact that the crystal seeds might have grown along some stacking pores at the beginning of the co-precipitation process of the transition metal hydroxide. The distribution of Ni, Mn and Co in the particle (Figs. 2b-d) was examined by energy dispersive x-ray spectroscopy (EDX). Compared with regular NMC spherical particles, EDX mapping of NMC lamella could reveal both inner and outer elemental distributions. The EDX maps of the Ni, Mn, and Co matched well each other, suggesting that the distribution of Ni, Mn and Co (Figs. 2b-d) is uniform throughout the material, suggesting a successful chemical synthesis of homogenous NMC particles. The EDX spectrum associated with the maps was shown in Fig. S3. Atomic ratios of Ni: Mn: Co were calculated from the metal $K\alpha$ peaks to be 17.6:1:1, which was consistent with ICP elemental analysis (Ni: Mn: Co = 88:6:6) shown in Table S2.

The $1\,\mu m$ NMC lamella was then milled to an ultrathin NMC cross section (<20 nm) and examined using at the atomic scale using a fifthorder aberration-corrected high-angle annular dark-field (HAADF) scanning transmission electron microscopy (STEM). Since the intensity of HAADF-STEM image is proportional to the atomic number (I $\propto Z^{1.7}$), transition metal atoms of Ni, Mn and Co will be much brighter than the light elements of oxygen and lithium. As shown in Fig. 2e and f, the HAADF-STEM image and its Fast Fourier Transform (FFT) clearly revealed the layered structure of transition metals in NMC at the atomicscale. (003) and (101) planes were observed in two directions with an angle of 79.5° on the [010] zone axis, which is consistent with the hexagonal α -NaFeO₂ type structure of NMC-111 [26]. The (003) planes had a d-spacing of 4.8 Å, similar to that of the reference NMC-111 (4.74 Å) whereas the (101) had a d-spacing of 2.6 Å, slightly larger than that of a reference NMC-111 (2.44 Å). Since the lattice parameter of Ni-rich NMC is 2.876 Å in the a and b directions, larger that of the NMC-111 reference (2.860 Å), the (101) lattice expansion of Ni-rich

NMC is likely due to the high Ni content and consistent with the shift to lower angles of the (101) facets in the powder XRD pattern (Fig. 1a). The corresponding crystal model (Fig. 2g) showed the projection of transition metals layers on the same [010] zone axis and is consistent with the layered structure in the STEM image.

The electrochemical characterization was carried out using pristine NMC and CF-NMC as cathodes, respectively, and lithium metal as the anode in coin cells. As shown Fig. 3a, during the initial charge/discharge profiles at 0.2 C from 2.8 to 4.3 V, CF-NMC delivered a nearly same discharge capacity (210 vs. 212 mA h/g) and a slightly better coulombic efficiency at the first cycle (90.1 vs. 89.8%), relative to the pristine NMC cathode. To investigate the discharge rate capability at various current densities, the cells were initially charged at 0.5 C. Fig. 3b presents the capacity retentions at various current rates from 0.2 C to 20 C between 2.8 and 4.3 V. The discharge capacities were similar at lower C rates for both pristine NMC and CF-NMC, but clear capacity differences increased gradually with the increasing rate. Noticeably, the rate capability for the CF-NMC sample was significantly better when compared to the pristine

Figs. 3c and 3d shows the discharge profiles of pristine NMC and CF-NMC materials at different current rates, respectively. Capacity differences became more evident at higher C rates, and these differences increased with increasing rates. The CF-NMC showed a relatively stable high capacity at both low and high C rates, when compared to the rapid decay in capacity of pristine NMC at higher C rates. The CF-NMC material maintained a remarkable capacity of 155 mA h/g at 5 C, relative to the much lower capacity of pristine NMC (89 mA h/g at 5 C). Furthermore, the CF-NMC cathode still delivered capacities of 137 and 95 mA h/g at the ultrahigh C-rates of 10 and 20 C, respectively, in contrast, the pristine NMC lost all of its capacity. In summary, the CF-NMC material delivered a significantly better capacity retention than the pristine NMC, particularly at high C rates. This might arise from the faster ionic and/or electronic diffusion and shorter migration paths at high rates, which benefited from the network structures.

The cycling performances of the CF-NMC and the pristine NMC cathodes were evaluated over the voltage range of 2.8 and 4.3 V at 0.5 C

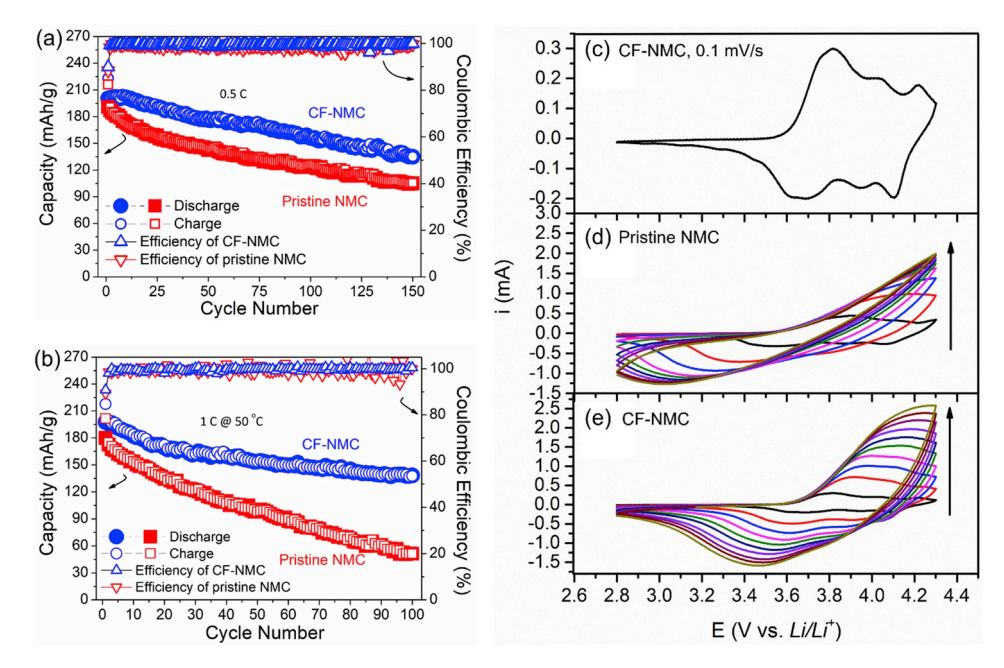


Fig. 4. (a) Cycling performance of CF-NMC and pristine NMC cells, up to 150 cycles between 2.8 and 4.3 V at 0.5 C at room temperature (25 °C). (b) Cycling performance of CF-NMC and pristine NMC cells at 1C at 50 °C. (c) CV profiles of a lithium half cell using CF-NMC as cathode at 0.1 mV/s. CVs of lithium half cells using (d) pristine NMC and (e) CF-NMC as cathodes arrows indicate increasing scan rates of 0.1, 0.3, 0.5, 0.7, 0.9, 1.1, 1.3, 1.5, 1.7 and 1.9 mV/s.

(Fig. 4a). The first discharge capacities of the CF-NMC and pristine NMC materials were calculated to 200 and 191 mAh/g, respectively. The capacity retention of the CF-NMC was 67.3% after 150 cycles, which was higher than that of the pristine NMC material (55.0% capacity retention after 150 cycles). The cycling performances of the CF-NMC and pristine NMC cathodes at an elevated temperature of 50 °C were also studied. As shown in Fig. 4b, the capacity of CF-NMC cathode lost 30.0% after 100 cycles, which was much less pronounced than that of pristine NMC electrodes (71.5% loss after 100 cycles). The dramatically better cycling stability and capacity retention of the CF-NMC material may be attributed to the synergistic effect of the larger specific surface area and the protection of the carbon fiber coating. Compared to the pristine NMC samples, the larger specific surface area of carbon fibers provides more transport paths for ions and/or electrons, and the carbon coating layer simultaneously prevents the inner oxide from reacting with HF in the electrolyte and agglomeration during electrochemical testing.

Cyclic voltammetry (CV) experiments in coin cells using pristine NMC and CF-NMC as cathode materials in lithium half-cells were performed to provide insights on the structural dynamics. Fig. 4c, presents the CV of a coin cell with CF-NMC as cathode that was cycled from 2.8 to 4.3 V at 0.1 mV/s. Three redox couples centered at 3.75, 3.99 and 4.17 V was clearly observed. A similar behavior was also observed in the charge/discharge profiles (Fig. 3a), as three plateaus are also present, corresponding to the redox couples observed in the CV. Such redox couples are characteristic of phase transitions, which have been extensively studied in LiNiO₂ [29] and LiNi_{1-x}Co_xO₂ (x = 0-0.3) [30,31]. These redox couples indicate phase transitions in CF-NMC from hexagonal (H₁) to monoclinic (M₁), monoclinic (M₁) to hexagonal (H₂) and hexagonal (H₂) to hexagonal (H₃), as the cell is charged from 2.8 to 4.3 V [29]. As shown in these studies, higher Ni contents are associated with more evident phase transitions in both CV and charge/discharge curves, indicating that such structural transitions are dominated by the LiNiO2 layered structure. CVs at different scan rates for pristine and CF-NMC were compared. From 0.1 mV/s to 1.9 mV/s, pristine NMC (Fig. 4d) clearly showed larger internal resistance when compared to CF-NMC (Fig. 4e). As the scan rate increased, the CF-NMC could capture the phase transitions up to ca. 1.1 mV/s, while for the pristine NMC, the transitions were barely visible at even the slowest scan rates, indicating the superior electronic conductivity provided by the use of the carbon fiber conductive network in CF-NMC.

3. Conclusions

In summary, we have prepared a carbon fiber interwoven $LiNi_{0.88}Mn_{0.06}Co_{0.06}O_2$ cathode (CF-NMC) material with enhanced rate capability and stability. The CF-NMC composites exhibited a higher capacity retention, better rate capability and more stable cyclic performance when compared to the pristine counterpart. The CF-NMC material also exhibited improved cycling performance when compared to the pristine sample, under both room temperature and elevated temperature (50 °C). The exceptionally high rate performance is most likely attributed to the faster ionic/electronic diffusion and shorter migration paths at high rate, which benefited from the carbon fiber network structure. The CF-NMC cathode material is practical and ready to use in electric vehicle applications which require low cost, high power, and long cycling performance especially at high operating temperatures.

Author contributions

†D. R. and Y. Y. contributed equally to this work. D.R. designed the material and performed the synthesis and battery tests. Y.Y. conducted the XRD, SEM, FIB-EDX and atomic-scale STEM imaging. L.S. performed the CV analysis. R.Z. performed the TG analysis.

Notes

The authors declare no competing financial interest.

Declaration of competing interest

The authors declare no competing financial interest.

Acknowledgments

This work made use of the Cornell Center for Materials Research Shared Facilities which are supported through the NSF MRSEC program (DMR-1719875).

Appendix A. Supplementary data

Supplementary data to this article can be found online at https://doi.org/10.1016/j.jpowsour.2019.227344.

References

- [1] V. Etacheri, R. Marom, R. Elazari, G. Salitra, D. Aurbach, Challenges in the development of advanced Li-ion batteries: a review, Energy Environ. Sci. 4 (2011) 3243–3262.
- [2] B. Scrosati, J. Garche, Lithium batteries: status, prospects and future, J. Power Sources 195 (2010) 2419–2430.
- [3] S.H. Ju, I.-S. Kang, Y.-S. Lee, W.-K. Shin, S. Kim, K. Shin, D.-W. Kim, Improvement of the cycling performance of LiNi_{0.6}Co_{0.2}Mn_{0.2}O₂ cathode active materials by a dual-conductive polymer coating, ACS Appl. Mater. Interfaces 6 (2014) 2546–2552.
- [4] T. Ohzuku, Y. Makimura, A possible alternative to LiCoO₂ for advanced lithium-ion batteries, Chem. Lett. 30 (2001) 744–745.
- [5] T. Ohzuku, Y. Makimura, Layered lithium insertion material of $LiCo_{1/3}Ni_{1/3}Mn_{1/3}$ $_{3}O_{2}$ for lithium-ion batteries, Chem. Lett. 30 (2001) 642–643.
- [6] P. Rozier, J.-M. Tarascon, Review—Li-Rich layered oxide cathodes for next-generation Li-ion batteries: chances and challenges, J. Electrochem. Soc. 162 (2015) A2490–A2499.
- [7] D.D. MacNeil, Z. Lu, J.R. Dahn, Structure and electrochemistry of Li $[Ni_xCo_{1-2x}Mn_x]O_2$ (0 \leq x \leq 1/2), J. Electrochem. Soc. 149 (2002) A1332–A1336.
- [8] S. Jouanneau, D.D. MacNeil, Z. Lu, S.D. Beattie, G. Murphy, J.R. Dahn, Structure and electrochemistry of Li[Ni_xCo_{1-2x}Mn_x]O₂ (0 ≤ x ≤1/2), J. Electrochem. Soc. 150 (2003) A1299–A1304.
- [9] J.K. Ngala, N.A. Chernova, M. Ma, M. Mamak, P.Y. Zavalij, M.S. Whittingham, The synthesis, characterization and electrochemical behavior of the layered LiNi_{0.4}Mn_{0.4}Co_{0.2}O₂ compound, J. Mater. Chem. 14 (2004) 214–220.
- [10] S.-J. Yoon, S.-T. Myung, Y.-K. Sun, Low temperature electrochemical properties of Li [Ni_xCo_yMn_{1.x.y.}]O₂ cathode materials for lithium-ion batteries, J. Electrochem. Soc. 161 (2014) A1514–A1520.
- [11] D. Ren, Y. Shen, Y. Yang, L. Shen, B.D.A. Levin, Y. Yu, D.A. Muller, H.D. Abruña, Systematic optimization of battery materials: key parameter optimization for the scalable synthesis of uniform, high-energy, and high stability LiNi_{0.6}Mn_{0.2}Co_{0.2}O₂ cathode material for lithium-ion batteries, ACS Appl. Mater. Interfaces 9 (2017) 35811–35819.
- [12] M. Zhang, H. Zhao, M. Tan, J. Liu, Y. Hu, S. Liu, X. Shu, H. Li, Q. Ran, J. Cai, X. Liu, Yttrium modified Ni-rich LiNi_{0.8}Co_{0.1}Mn_{0.1}O₂ with enhanced electrochemical performance as high energy density cathode material at 4.5 V high voltage, J. Alloy. Comp. 774 (2019) 82–92.
- [13] Q. Fan, S. Yang, J. Liu, H. Liu, K. Lin, R. Liu, C. Hong, L. Liu, Y. Chen, K. An, P. Liu, Z. Shi, Y. Yang, Mixed-conducting interlayer boosting the electrochemical performance of Ni-rich layered oxide cathode materials for lithium ion batteries, J. Power Sources 421 (2019) 91–99.
- [14] Y. Su, G. Chen, L. Chen, W. Li, Q. Zhang, Z. Yang, Y. Lu, L. Bao, J. Tan, R. Chen, S. Chen, F. Wu, Exposing the {010} planes by oriented self-assembly with

- nanosheets to improve the electrochemical performances of Ni-rich Li $[Ni_{0.8}Co_{0.1}Mn_{0.1}]O_2$ microspheres, ACS Appl. Mater. Interfaces 10 (2018) 6407–6414.
- [15] P. Yan, J. Zheng, J. Liu, B. Wang, X. Cheng, Y. Zhang, X. Sun, C. Wang, J.-G. Zhang, Tailoring grain boundary structures and chemistry of Ni-rich layered cathodes for enhanced cycle stability of lithium-ion batteries, Nat. Energy 3 (2018) 600–605.
- [16] J. Zheng, P. Yan, L. Estevez, C. Wang, J.-G. Zhang, Effect of Calcination Temperature on the Electrochemical Properties of Nickel-rich LiNi_{0.76}Mn_{0.14}Co_{0.10}O₂ Cathodes for Lithium-Ion Batteries 49 (2018) 538–548.
- [17] H.-J. Noh, S. Youn, C.S. Yoon, Y.-K. Sun, Comparison of the structural and electrochemical properties of layered Li[Ni_xCo_yMn_z]O₂ (x = 1/3, 0.5, 0.6, 0.7, 0.8 and 0.85) cathode material for lithium-ion batteries, J. Power Sources 233 (2013) 121–130.
- [18] C. Ban, N.A. Chernova, M.S. Whittingham, Electrospun nano-vanadium pentoxide cathode, Electrochem. Commun. 11 (2009) 522–525.
- [19] J. Liu, Q. Wang, B. Reeja-Jayan, A. Manthiram, Carbon-coated high capacity layered Li[Li_{0. 2}Mn_{0. 54}Ni_{0. 13}Co_{0. 13}]O₂ cathodes, Electrochem. Commun. 12 (2010) 750–753.
- [20] Z. Chen, J.R. Dahn, Reducing carbon in LiFePO₄/C composite electrodes to maximize specific energy, volumetric energy, and tap density, J. Electrochem. Soc. 149 (2002) A1184–A1189.
- [21] J. Jamnik, J. Maier, Nanocrystallinity effects in lithium battery materials: aspects of nano-ionics, Part IV, Phys. Chem. Chem. Phys. 5 (2003) 5215–5220.
- [22] A.S. Aricò, P. Bruce, B. Scrosati, J.-M. Tarascon, W. van Schalkwijk, Nanostructured materials for advanced energy conversion and storage devices, Nat. Mater. 4 (2005) 366–377.
- [23] L.A. Riley, S.V. Atta, A.S. Cavanagh, Y. Yan, S.M. George, P. Liu, A.C. Dillon, S.-H. Lee, Electrochemical effects of ALD surface modification on combustion synthesized LiNi_{1/3}Mn_{1/3}Co_{1/3}O₂ as a layered-cathode material, J. Power Sources 196 (2011) 3317–3324.
- [24] S.-T. Myung, K. Izumi, S. Komaba, H. Yashiro, H.J. Bang, Y.-K. Sun, N. Kumagai, Functionality of oxide coating for Li[Li_{0.05}Ni_{0.4}Co_{0.15}Mn_{0.4}]O₂ as positive electrode materials for lithium-ion secondary batteries, J. Phys. Chem. C 111 (2007) 4061–4067.
- [25] J.-Z. Kong, C. Ren, G.-A. Tai, X. Zhang, A.-D. Li, D. Wu, H. Li, F. Zhou, Ultrathin ZnO coating for improved electrochemical performance of LiNi_{0.5}Co_{0.2}Mn_{0.3}O₂ cathode material, J. Power Sources 266 (2014) 433–439.
- [26] S.-C. Yin, Y.-H. Rho, I. Swainson, L.F. Nazar, X-ray/neutron diffraction and electrochemical studies of lithium de/re-intercalation in $\text{Li}_{1-x}\text{Co}_{1/3}\text{Ni}_{1/3}\text{Mn}_{1/3}\text{O}_2$ (x = 0 \rightarrow 1), Chem. Mater. 18 (2006) 1901–1910.
- [27] A. Rougier, P. Gravereau, C. Delmas, Optimization of the composition of the Li₁₋₂Ni₁₊₂O₂ electrode materials: structural, magnetic, and electrochemical studies, J. Electrochem. Soc. 143 (1996) 1168–1175.
- [28] K. Kang, G. Ceder, Factors that affect Li mobility in layered lithium transition metal oxides, Phys. Rev. B 74 (2006) 94105.
- [29] W. Li, J.N. Reimers, J.R. Dahn, In situ X-ray diffraction and electrochemical studies of Li_{1-x}NiO₂, Solid State Ion. 67 (1993) 123–130.
- [30] J. Cho, H. Jung, Y. Park, G. Kim, H.S. Lim, Electrochemical properties and thermal stability of LiNi_{1-x}Co_xO₂ cathode materials, J. Electrochem. Soc. 147 (2000) 15–20.
- [31] J. Cho, T.-J. Kim, Y.J. Kim, B. Park, High-performance ZrO₂-coated LiNiO₂ cathode material, Electrochem. Solid State Lett. 4 (2001) A159–A161.